Nano-scale electronic structure of strongly correlated electron systems

Tromp, W.O.

1 Introduction

1.1 Complexity in Strongly Correlated Electron Systems

One of the oldest questions in science, dating back to at least as far back as Leucippus & Democritus in the 5th century BCE[1], is "What is matter made of?". This question has slowly morphed into a way of thinking, a method of tackling new problems: the reductionist approach. When faced with a system of unknown nature, physicists very naturally ask themselves what are the building blocks, in the hope that the properties of the building blocks easily translate into properties of the larger system. How those building blocks fit together, the glue that binds them, is often only a secondary consideration.

Perhaps no field of research embodies this approach as well as condensed matter physics. The building blocks here are the atoms forming the lattice, and the electrons moving through it. The approach of neglecting or heavily approximating the interactions between the building blocks is a necessity for an otherwise intractable problem. A centimetre sized piece of material is made up of 10^{23} atoms and electrons! Tracking every interaction among them is simply impossible. The field, therefore has a long history of approximations to deal with this problem, with successes some might call unreasonable. For example, even the Fermi gas, where the lattice is completely ignored together with any interaction between electrons, already has some of the essential features, such as a parabolic dispersion and a Fermi surface.

Departing from there each new interaction treated properly adds a new level of detail, but they all share a common theme: finding a particular angle to the problem so that the language of single particles still applies. For example, when treating the interactions between electrons and lattice vibrations, or phonons, one that the system still very much looks like free electrons, albeit with a modified dispersion relation for energies below the phonon frequency[2]. This strategy forms the foundation of much of the field and its application, though particularly electron-electron interactions are more stubborn to this approach.

In recent years condensed matter physicists have started asking questions moving away from this approach, in part motivated by the challenges posed by electron-electron interactions. A question like "Where does complexity come from?"[3-5] appears to be better suited for the category of systems scientists increasingly deal with, often called strongly correlated systems, where the

older approach no longer seems applicable. In these cases, the interactions, most commonly electron-electron interactions, are so dominant that the language of single electrons is no longer suitable. The physics of such a system are often emergent of collective phenomena, as they only appear when a large number of particles interact with each other. Properties of such systems can vary wildly, summarized beautifully by Philip Anderson: More is Different[3]. For example, electrons can freeze themselves in place in what should be a good metal[6] (Mott insulators), single particles can seize existing altogether[7] (strange metals), or the system shows behavior more associated with bosons[8] (superconductivity) or something in between called anyons[9].

One of the core concepts of condensed matter physics takes a rather peculiar place in this view: the quasi-particle. This concept is born from Landau's Fermi Liquid theory stating (rather simplified) that in the presence of interactions a system of electrons on a lattice can often be mapped back to a single particle physics of newly defined quasi-particles, provided the interactions aren't too strong. What those quasi-particles are depends on the exact system and nature of interactions. This is quite remarkable! The applicability of single particle physics extends farther than naively expected based on the number of particles involved. Still, this is not quite the victory for the reductionist approach as it seems, or perhaps just a surface level victory. Rather, the properties of a quasi-particle can be quite far removed from those of a regular electron. There is a whole zoo of quasi-particles that physicists have studied: plasmons, anyons, holons, basically anything ending with –on. It is this gap between regular electrons and quasi-particles, and the zoo of possible quasi-particles, where many-body physics most often shows itself and which a reductionist view often struggles to fill. In this sense, the quasi-particle itself is the emergent phenomenon. And yet there are limits to Fermi Liquid theory. For example, in the copper-oxide superconductors the concept of quasi-particles is certainly useful, but it doesn't cover the full story and sometimes seemingly does not even apply at all. Exactly how to understand and describe the copper-oxide superconductors is one of the major challenges of condensed matter physics.

1.2 Copper-Oxide Superconductors

One of the most notorious examples of emergent phenomena in condensed matter physics, and a primary subject of this thesis, are the copper oxide,

or cuprate, high-temperature superconductors. These superconductors are composed of alternating layers of CuO square lattices, where the charge carriers reside, and insulating buffer layers (see **Fig. 1.1a**). The electronic state underlying these compounds is a Mott insulator, itself a prime example of a system where interactions dominate the properties. The insulating state arises when the CuO square lattice, schematically shown in **Fig. 1.1b** has one carrier per unit cell, i.e. the lattice is half-filled. Without any interactions the half-filled square lattice would yield a metallic state. The cuprate superconductors however feature a strong on-site electron-electron repulsion, often called U, meaning that the presence of two electrons on a single lattice site is penalized by an energy cost U. This energy scale is in competition with the natural tendency of electrons to delocalize, parametrized by the hopping energy t. If the repulsion U is much stronger than the hopping term t the electrons are frozen in place, unable to leave their lattice site. The result is a strongly insulating state. Additionally, these electrons are arranged antiferromagnetically. This is the result of the Pauli principle adding an extra energy cost for virtual hopping events were the electrons to have a ferromagnetic alignment.

The seemingly odd choice to start a discussion of a compound family most famous for their superconductivity by discussing a strongly insulating state is a sign for things to come when we dope the Mott insulating state (for the purposes of this thesis hole-dope specifically). The insulating state quickly melts with doping, and superconductivity emerges (see **Fig. 1.2a**). One important feature of the superconducting state is its d-wave symmetry[7], meaning the wavefunction flips sign upon 90 degree rotation. As a result, the superconducting gap has nodes where it goes to zero, lying on the diagonals in k-space. This splits k-space into two regions (**Fig. 1.2b**): the nodal direction in the neighborhood of the diagonals, and the anti-nodes near the Brillouin zone edges $k = (\pm\pi/a,0)$ and $k = (0,\pm\pi/a)$. Another important feature of cuprates is the strong spatial inhomogeneity of the electronic state. This can be attributed to Mott physics still being at play, despite the insulating state being suppressed. From this emergences a disposition towards phase separation and the emergence of multiple ordered states on extremely short length scales.

In the region of the phase diagram where T_c is increasing with doping, called the *underdoped* regime, the system is dominated by another salient feature called the pseudogap. This phase features a partial gap, with anti-nodal states being strongly suppressed. As a result, there is no conventional Fermi surface:

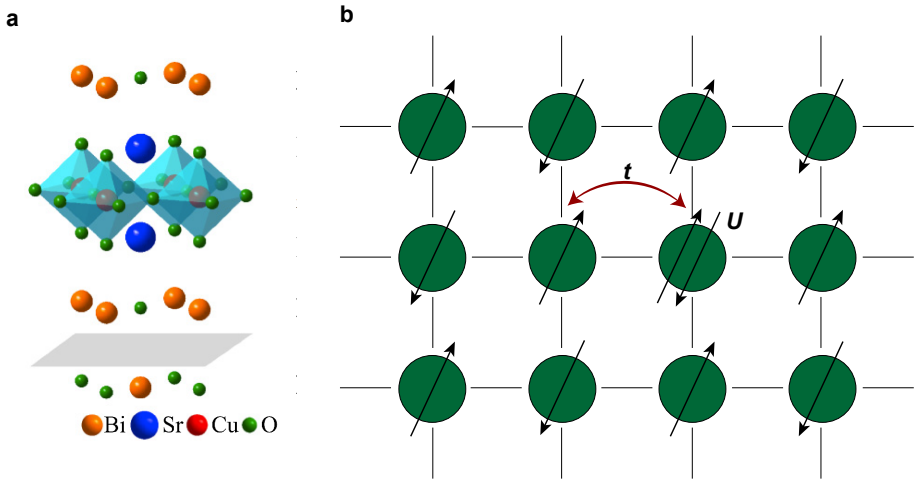

Figure 1.1: Cuprate unit cell.
a) *The unit cell of the cuprate superconductor $Bi_2Sr_2CuO_{6+\delta}$ (Bi2201), subject of Chapters 3 & 4. The charge carriers reside in the CuO planes, while the BiO and SrO planes act as insulating buffer layers hosting the dopants. Image adapted from Ref.10.* ***b)*** *Schematic of of a Mott insulator, showing one electron per unit cell with spins aligned antiferromagnetically. When the energy cost of a doubly occupied lattice site U is larger than the hopping energy t the system turns insulating.*

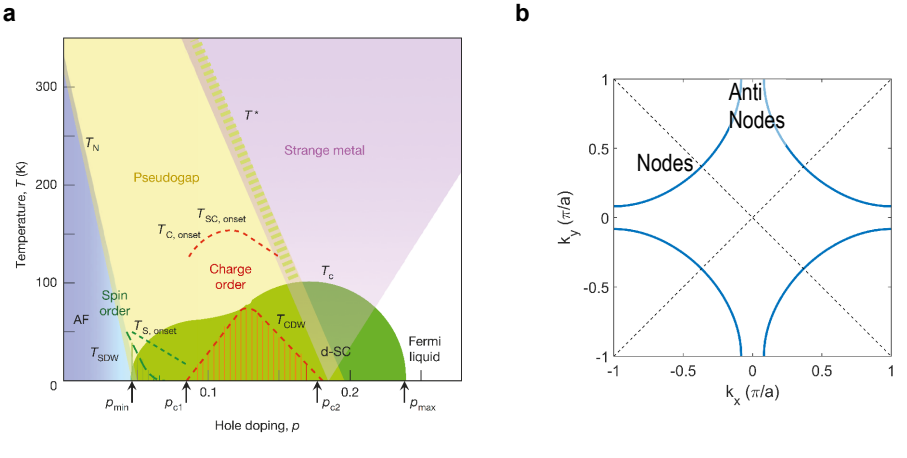

Figure 1.2 Electronic phases of cuprate.
a) *Phase diagram of the many different electronic phases cuprates have been shown to host. Image adapted from Ref. 7.* ***b)*** *Sketch of the cuprate Fermi surface. The Brillouin zone diagonals (dashed lines) divide the Fermi surface in two parts: the nodal region, where the gap function goes to zero, and the anti-nodal region, where the gap function reaches its maximum.*

near the anti-nodes there are no discernable quasiparticles in spectroscopy[11-13], while near the nodes there are still quasiparticles present at E_F. When looking at the Fermi level with momentum resolved spectroscopy, one finds four sets of disconnected states near the nodes called Fermi arcs. Complicating matters further, this phase also features a multitude of different ordered phases[14-19] and possibly precursor pairing, where Cooper pairs have already formed but have not yet condensed into a single state[20-23]. How all of the pieces of puzzle fit together is still unknown, leaving the nature of the pseudogap state still an open question.

At a doping level of 16% (referred to as optimal doping) the T_c reaches a maximum. In this regime the pseudogap state gives way to a perhaps even more poorly understood state. This is the so-called strange metal phase. It is characterized by a linear in temperature resistivity over the full range spanning from T_c to the highest measured temperatures[24,25]. This particular temperature dependence is present over a broad doping range, even at low temperatures[26,27]. This is in contrast to quantum critical behavior, where this phenomenology would reduce down to a single doping point at zero temperature[28]. Perhaps the strangest features of this state is that it seems to no longer feature coherent quasi-particles[29,30]. Instead, charge is carried by a fully incoherent fluid. One framework to model this state is based around the AdS/CFT correspondence from string theory[7,31,32]. With this correspondence a class of quantum theories (so-called conformal field theories, or CFTs) can be mapped onto a gravitational problem of a particular geometry (problems in an anti de sitter space, or AdS) in one higher spatial dimension. The metallic states emerging from this construction share some similarities with the strange metal behavior found in the cuprates. A particularly interesting prediction is that transport in this state features hydrodynamic flow as opposed to the ohmic transport of regular metals[33-35]. Additionally, the incoherent fluid is proposed to have an extremely low viscosity, raising the possibility of turbulent flow even on the nanometer scale. This is all despite the high levels of disorder cuprates are known to have[35].

When increasing the doping level even further into the overdoped regime, the T_c drops again. At some point a Fermi liquid metallic state is recovered, as is evidenced by the visibility of a full Fermi surface in spectroscopy[11,30,36,37] and the observation of quantum oscillations[38,39]. The reversion back to a more conventional Fermi liquid is not without its own mysteries however. For example, signs of incoherent carriers associated with the strange metal phase

have been found even when T_c has dropped to nearly zero[27]. Furthermore, the decrease of T_c also features a drop of the number of condensed carriers, the superfluid density[40-42]. In more regular superconductors, the superfluid density scales with the total number of carriers in the system. This means that as the doping increases, i.e. more carriers are introduced, the superfluid density should go up, whereas the exact opposite is found to occur in the cuprates. Instead, an increasingly large number of uncondensed carriers emerge with overdoping[43-45]. Furthermore, signs of fluctuating superconductivity above T_c have been seen through the persistence of a gap above T_c[46-48] and through AC and DC transport signatures[22,49]. An important role in these phenomena is played by disorder[50,51], which naturally increases as more dopants are introduced in the overdoped regime.

One proposal to explain these observations involving disorder is the formation of a granular superconductor[52,53]. In such a system superconducting islands are separated by metallic regions. A key ingredient of this proposal is enhanced anti-nodal scattering due to a Van Hove singularity (vHS) close to Fermi level at the anti-nodes. Neighboring anti-nodes have opposite sign due to the d-wave symmetry. This particular type of scattering therefore breaks Cooper pairs. The presence of the Van Hove singularity enhances this scattering to the point it locally breaks down superconductivity all together, leaving behind a metallic region. The existence of the metallic regions would explain the anomalously low superfluid and uncondensed carriers, as parts of the system is not superconducting at all. The superconducting regions of the system become more dilute with increased doping. At some point, the macroscopic properties of the system are no longer a consequence the properties of the wavefunction within a single region, but rather a consequence of the coupling of these regions to each other. Finally, when the coupling becomes sufficiently weak, or when the superconducting islands become sufficiently dilute, macroscopic superconductivity has vanished. Some traces of superconductivity may however still remain in this otherwise metallic state.

Complicating this proposal, or the breakdown of overdoped superconductivity in general, are observations of additional ordered states, specifically ferromagnetic fluctuations[54,55] and charge order near the edge of the superconducting dome[56-58]. The latter is of particular interest as it has only been observed for doping levels around the level where superconductivity vanishes altogether. Additionally, the wavelength observed in real space

suggests a close tie to the vHS which exists near the Fermi level in the same doping range. It should be noted however that RIXS experiments disagree on the charge order wavelength[57], and, while visible in real space, STM results find no clear feature in momentum space[58]. How this relates to the breakdown of superconductivity remains an open question.

1.3 Scanning Tunneling Microscopy

A common feature of strongly correlated electron systems is their nanoscale electronic inhomogeneity[59-61]. A careful study of these systems therefore requires an accurate mapping of their real space electronic structure on an atomic scale. It is for this purpose that scanning tunneling microscopy, or STM, is invented[62].

The principle of operation for STM is quantum tunneling of electrons between the sample and an atomically sharp tip used to study it[63]. When the two are brought together sufficiently close to each other (typically meaning less than a nm) and a voltage is applied between them, called the bias voltage, electrons can jump between them without them being in physical contact (see **Fig. 1.3a**). The current that starts to flow as a result can be used to both image the surface of the sample, and measure the DOS directly below the tip.

The bias voltage shifts the Fermi levels of the tip and sample with respect to each other (**Fig 1.3b**) so that electron move from the occupied states on one side to the unoccupied states on the other (which side is which depends on the sign of the applied voltage). The resulting current is then given by the overlap of the occupied DOS on one side and the unoccupied DOS on the other:

$$I(V_b) = \frac{4\pi e}{\hbar} \int_{-\infty}^{+\infty} |M|^2 g_t(\epsilon - eV_b) g_s(\epsilon) [f(\epsilon) - f(\epsilon - eV_b)] d\epsilon \quad (1.1)$$

Where $g_{t,s}$ denotes the density of states of the tip and the sample, f the Fermi-Dirac distribution, V_b the bias voltage, and M the tunneling matrix elements controlled by the details of the tunneling process. Often, simplifications can be made to this equation by assuming the density of states of the tip to be constant in energy (as can be done by choosing the appropriate material for the STM tip), and the Fermi-Dirac functions to be step-functions. The latter is only valid at low temperatures, a point we will come back to when

discussing tunneling spectroscopy and energy resolution. Doing this reduces the expression for the tunneling current to:

$$I(V_b) \propto \frac{4\pi e}{\hbar} g_t |M|^2 \int_0^{\epsilon V_b} g_s(\epsilon) d\epsilon \tag{1.2}$$

Where the step-function shape of the Fermi-Dirac distribution was used to change the integration bounds. For simplicity's sake M is also assumed to be constant in energy. The matrix elements M are largely determined by the overlap of the orbitals of the tip and the sample, which is often energy independent. The orbital overlap decays exponentially with the distance z between tip and sample, meaning the tunneling current is extremely sensitive to the distance between tip and sample. This distance is controlled by a feedback mechanism. The tunneling current is constantly recorded and the tip height constantly adjusted so that the current stays constant. When the tip is moved across the surface, an image of the surface is reconstructed by recording the changes in the tip height needed to keep the current constant. Despite the feedback loop, STM is still extremely sensitive to outside influences disturbing the tip-sample distance, such as vibrations or sound waves. New STM setups are continuously being developed to minimize outside disturbances, with

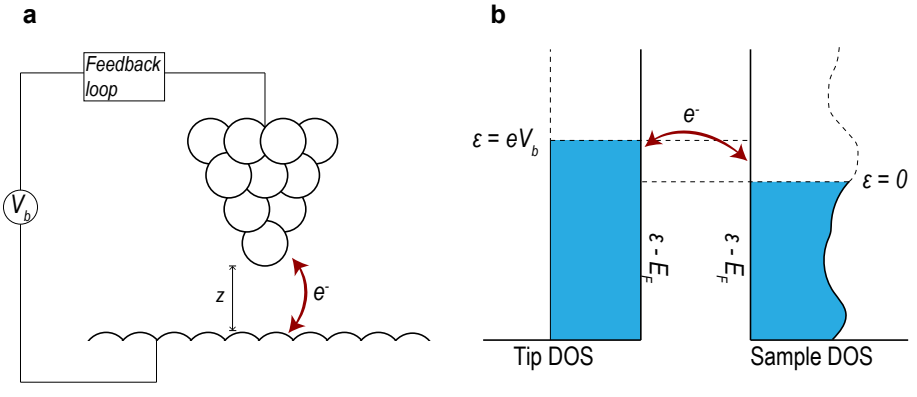

Figure 1.3 Basics of STM.
a) *Schematic of the tip-sample system for STM. At sufficiently close distance z between tip and sample, regulated via the feedback loop, electrons can jump the gap when a bias voltage V_b is applied.* ***b)*** *Diagram of the DOS on the tip and sample sides. Current can flow between the tip and the sample when electrons can jump from occupied states on one side (here the tip) to unoccupied sides on the other side (here the sample). The total current is proportional to the size of the tunneling window given by eV_b and the total number of states inside said window.*

the state-of-the-art system used for the majority of this thesis' experiments reaching a vibration level[64] as low as 6 fm $Hz^{-1/2}$.

Accessing the DOS of the sample, i.e. doing tunneling spectroscopy, is done by taking the derivative of eq. 1.2 with respect to the bias voltage V_b. This yields the following expression:

$$\frac{\partial I}{\partial V_b}(V_b) = \frac{4\pi e}{\hbar}|M|^2 g_t g_s(\epsilon V_b) \tag{1.3}$$

Measuring this quantity as a function of V_b is called a dI/dV spectrum, giving direct information about the local DOS (or LDOS) of the sample. To do this, the tip position above the sample is stabilized using the feedback loop at a current I_S and voltage V_S called the setup current and voltage. The feedback is then switched off and the bias voltage is swept while recording the tunneling current. The dI/dV could of course then be calculated through numerical differentiation. Doing so however enhances the noise in a spectrum. Instead, the dI/dV is directly measured by adding a small modulation ΔV at a given frequency to the bias voltage, and measuring the resulting oscillations ΔI at that frequency using a lock-in amplifier. The ratio $\Delta I/\Delta V$ gives then the DOS in a window ΔV around V_b. After the sweep is finished the feedback is enabled again so the tip can safely be moved to another location.

All of the above is combined into a single technique called Scanning Tunneling Spectroscopy (STS, although spectroscopic imaging STM or SI-STM is also used). Here, a finely spaced grid of 10^4-10^5 points or pixels is defined on a small section of sample surface (in the range of 10x10 nm). At each point both the tip height and the LDOS are measured by first stabilizing the tip position with feedback on and then measuring the dI/dV. As such, a 2D map of the surface is created simultaneously with a 3D map of the electronic structure, where the third dimension are the energies at which the LDOS was measured. The ability to measure the electronic structure with such a high spatial resolution is especially well suited for studying strongly correlated systems which naturally tend to inhomogeneous electronic structures.

The energy resolution of spectroscopic imaging is largely set by how the approximation of Fermi-Dirac distributions as step-functions works. Going through the derivation more carefully, one finds that the expression for dI/dV contains a derivative of the Fermi-Dirac distribution, which is a Gaussian with

a FWHM of $3.53k_bT$. Furthermore, the modulation used to measure dI/dV adds its own resolution given by the amplitude of the modulation. These two values add quadratically to give the total resolution. For example at a temperature of 4.2K and a modulation of 1.5mV, the total resolution is 2.58meV.

While STS is most often used to image the real space electronic structure, it can also measure a momentum resolved structure with a technique called Quasi-Particle Interference or QPI. This technique makes use of the standing waves around impurities or defects in the material that STS can observe[65,66], caused by electrons scattering off the defects (see **Fig. 1.4a** for a simulation) An

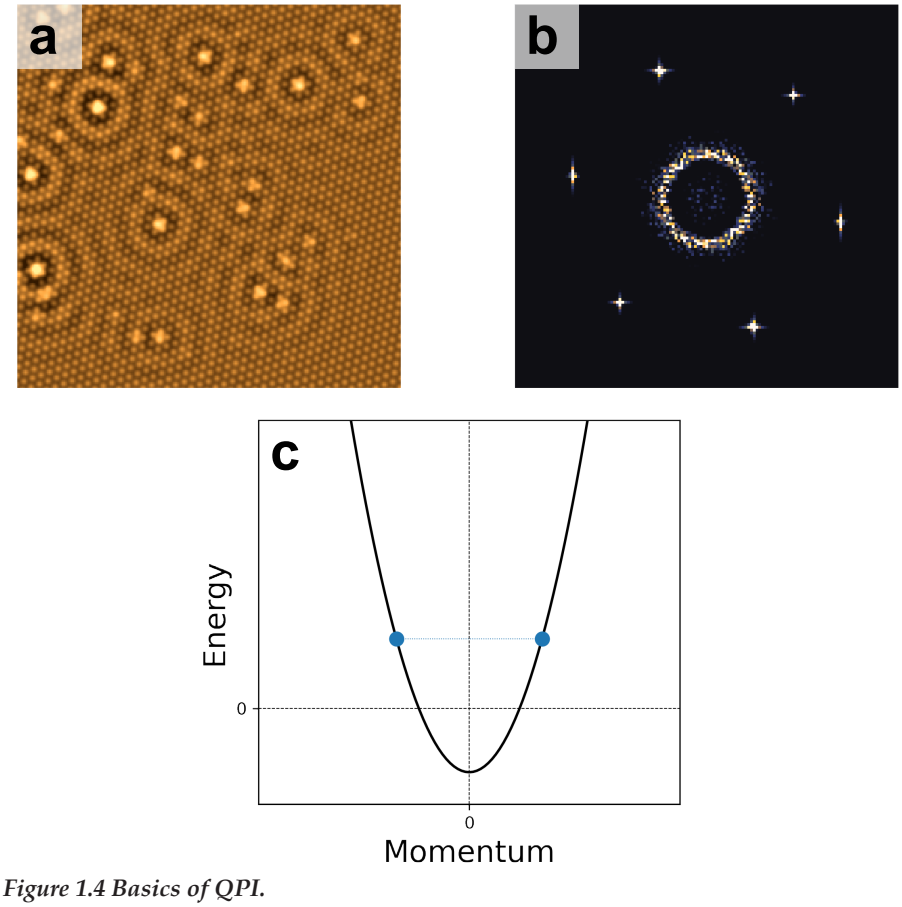

Figure 1.4 Basics of QPI.
a) *Simulation of a Cu(111) lattice with defects showing QPI rings from electron interference.* ***b)*** *Fourier transform of* ***a)*** *clearly showing 6 isolated Bragg peaks from the lattice and the a ring-shaped feature from the QPI waves.* ***c)*** *The wavevector of the QPI waves, and with it the size of the ring in* ***b)****, is determined by bandstructure (here parabolic) of the system. The blue dots show the momentum of the carriers at the energy used for* ***a,b)****. Credit: K. Fujita.*

incoming electron with momentum $\boldsymbol{k}_1$ and energy $\varepsilon(\boldsymbol{k}_1)$ will scatter into a final state with momentum $\boldsymbol{k}_2$ and energy $\varepsilon(\boldsymbol{k}_2) = \varepsilon(\boldsymbol{k}_1)$. The interference between these states causes an oscillation in the DOS with a wavevector $\boldsymbol{q} = \boldsymbol{k}_1 - \boldsymbol{k}_2$. The value of the wavevector $\boldsymbol{q}$ can be measured by imaging the oscillation pattern in real space and taking a Fourier transform.

For the case that the system has a only a single band electrons will simply scatter from one side of the Fermi surface to the other: $\boldsymbol{q} = \boldsymbol{k}_F - (-\boldsymbol{k}_F) = 2\boldsymbol{k}_F$. Measuring $\boldsymbol{q}$ as a function of energy then directly yields the bandstructure of the material (see **Fig. 1.4b, c**). For multiband systems, the situation is more complicated. Not only are there multiple values for $\boldsymbol{q} = 2\boldsymbol{k}_F$, one for each band, but also multiple different $\boldsymbol{q}$'s resulting from interband scattering. While in principle tracking the dispersions of these scattering vectors contains all the information on the bandstructure, extracting the exact dispersion is often impossible without some prior knowledge of the bandstructure. More generally, QPI will measure the scattering vector between states with a high joint density of states (JDOS). These are often states whose constant energy contours are parallel[67,68] or parts of the bandstructure which feature a flat dispersion which increases the DOS, a useful fact for determining gapped bandstructures[69,70].

Viewing QPI through the lens of the JDOS gives a way to better approximate what a QPI measurement will look like. To do this, it is most useful not to think in terms of DOS but of the spectral function $A(\boldsymbol{k},\omega)$. This quantity is a generalized version of the DOS suitable for correlated systems, giving the probability there is a quasi-particle excitation with momentum $\boldsymbol{k}$ and energy ω[71]. The JDOS is then well approximated by:

$$JDOS(\mathbf{q},\omega) = \int A(\mathbf{k},\omega)A(\mathbf{k}+\mathbf{q},\omega)d\mathbf{k} \tag{1.4}$$

Although simple, this allows for quick estimation of QPI measurements, especially given the fact that the spectral function $A(\boldsymbol{k},\omega)$ for occupied states is directly accessible in ARPES measurements[72]. By taking the autocorrelation of constant energy ARPES measurements, or results from the computational method for bandstructure of choice, a good first guess for the QPI signal is obtained. Of course more complicated, and more precise, methods to calculate QPI patterns exist[67,73], but the autocorrelation method is often good enough to identify the visible scattering vectors without the need of any further aids.

High quality QPI measurements push the technique of STS to its limits, primarily due to the length of such a measurement. The field of view used needs to be large enough, as this directly sets the resolution in $\boldsymbol{q}$. Still, the spectroscopy grid needs to be fine enough to resolve features with higher $\boldsymbol{q}$. Preferably, the atomic lattice is still resolved, as the subsequent Bragg peaks in the QPI signal are ideal for calibrating lengths of scattering vectors. Lastly, the signal-to-noise ratio of each spectrum needs to sufficient so that the oscillations in the LDOS are not washed out. The result is that QPI measurements take a long time, the ones presented in this thesis often taking 2-3 days, occasionally up to 5 days. As such, stability of the STM setup is paramount, both in terms of temperature stability and vibration isolation.

Even when these issues are properly addressed, QPI measurements are prone to artifacts, the most important of which is the setup effect[74,75]. This is a direct consequence of the choice to enable the feedback loop again after measuring each dI/dV spectrum. This introduces a normalization factor into the spectrum, which can be thought of as a 'leak' of the signal at the setup bias into the signal at other bias levels. For QPI measurements, this results in a constant-in-$\boldsymbol{q}$, or non-dispersive, signal in the measurement[75]. The exact shape and position of the artifact depends on what the visible $\boldsymbol{q}$-vector is at the setup bias. Armed with this knowledge, it is in principle possible to design the QPI measurement in such a way that there is no setup effect present, although this can require impractical values for the setup bias.

1.4 Outline of this Thesis

In this thesis we will closely examine how we study strongly correlated systems, and apply that knowledge to the study of cuprate superconductors. Finally, we propose new experiments to explore the properties of strongly correlated systems. This thesis is structured as follows:

In Chapter 2 we study how electronic structures are determined by studying a prototypical example of a correlated 2D Fermi Liquid, Sr_2RhO_4. We do this by applying three commonly used spectroscopic techniques, STS, ARPES, and quantum oscillations, and find them to be in good agreement. We argue that discrepancies between these methods in other systems are a reflection of the physics of those systems.

In Chapters 3 & 4, we study the electronic structure of the overdoped cuprate $(Pb,Bi)_2Sr_2CuO_{6+\delta}$, both in real space and in momentum space, using STS and QPI measurements. In Chapter 3, we study the real space structure by tracking the evolution of the superconducting gap across and beyond the superconducting dome. We find that the magnitude of the spectroscopic gap no longer follows the superconducting dome, and instead levels out. Furthermore, we find that a metallic matrix forms and grows with increasing doping on the nm scale in this system, and that the mechanism of pair breaking in this system falls outside the scope of mean field theories. In Chapter 4 we employ a combination of QPI and state-of-the-art machine learning noise suppression to probe the momentum space structure of $(Pb,Bi)_2Sr_2CuO_{6+\delta}$. We find an anti-nodal band rigidly shifting with doping, in line with earlier results. We also observe the bending of the band due to the gap and find shoulder-like features near the gap edge suggesting the presence of an additional density wave in these samples.

Finally, in Chapter 5 we discuss how strong correlations between electrons can give rise to a rare form of transport called hydrodynamic transport. We model the transport behavior in this regime for an experiment designed to detect hydrodynamic transport using the Navier-Stokes equation modified to include disorder effects. We carefully calculate the expected signal for this experiment for the Fermi Liquid normal state of the unconventional superconductor Sr_2RuO_4, and find a crossover between Ohmic and hydrodynamic transport over a range of disorder levels. Finally, we discuss the application of this experiment to the cuprate strange metal phase, which has been proposed to show hydrodynamical behavior with an extremely low viscosity. We show that the same experiment will show only Ohmic behavior due to the combination of disorder and low viscosity in cuprate strange metals.

1.5 References

[1] Berryman, S. Democritus, in *The Stanford Encyclopedia of Philosophy*. (Metaphysics Research Lab, Stanford University, 2016).

[2] Ashcroft, N. W. & Mermin, N. D. *Solid State Physics*. (Brooks/Cole, Cengage Learning, 1976).

[3] P. W. Anderson, More is Different. *Science* **177**, 393–396 (1972).

[4] Laughlin, R. B. & Pines, D. The Theory of Everything. *Proc. Natl. Acad. Sci.* **97**, 28–31 (1999).

[5] Elbio, D. Complexity in Strongly Correlated Systems. *Science* **309**, 257–262 (2005).

[6] Imada, M., Fujimori, A. & Tokura, Y. Metal-insulator transitions. *Rev. Mod. Phys.* **70**, 1039–1263 (1998).

[7] Keimer, B., Kivelson, S. A., Norman, M. R., Uchida, S. & Zaanen, J. From quantum matter to high-temperature superconductivity in copper oxides. *Nature* **518**, 179–186 (2015).

[8] Bardeen, J., Cooper, L. N. & Schrieffer, J. R. Theory of Superconductivity. *Phys. Rev.* **108**, 1175–1204, (1957).

[9] Nakamura, J., Liang, S., Gardner, G. C. & Manfra, M. J. Direct observation of anyonic braiding statistics. *Nat. Phys.* **16,** 931–936 (2020).

[10] Lv, Y. F. *et al.* Electronic structure of the ingredient planes of the cuprate superconductor $Bi_2Sr_2CuO_{6+\delta}$: A comparison study with $Bi_2Sr_2CaCu_2O_{8+\delta}$. *Phys. Rev. B* **93**, 140504 (2016).

[11] He, Y. *et al.* Fermi Surface and Pseudogap Evolution in a Cuprate Superconductor. *Science* **344,** 612–616 (2014).

[12] Hashimoto, M. *et al.* Direct spectroscopic evidence for phase competition between the pseudogap and superconductivity in $Bi_2Sr_2CaCu_2O_{8+\delta}$. *Nat. Phys.* **10**, 483–495 (2014).

[13] Vishik, I. M. Photoemission perspective on pseudogap , superconducting fluctuations , and charge order in cuprates : a review of recent progress *Reports Prog. Phys.* **81**, 062501 (2018).

[14] Fujita, M., Goka, H., Yamada, K., Tranquada, J. M. & Regnault, L. P. Stripe order, depinning, and fluctuations in $La_{1.875}Ba_{0.125}CuO_4$ and $La_{1.875}Ba_{0.075}Sr_{0.050}CuO_4$. *Phys. Rev. B* **70**, 104517 (2004).

[15] Kohsaka, Y. *et al.* An intrinsic bond-centered electronic glass with unidirectional domains in underdoped cuprates. *Science* **315**, 1380–1385 (2007).

[16] Lawler, M. J. *et al.* Intra-unit-cell electronic nematicity of the high-T c copper-oxide pseudogap states. *Nature* **466**, 347–351 (2010).

[17] Ghiringhelli, G. *et al.* Long-Range Incommensurate Charge Fluctuations in $(Y,Nd)Ba_2Cu_3O_{6+x}$. *Science* **337**, 821–825 (2012).

[18] Hamidian, M. H. *et al.* Detection of a Cooper-pair density wave in $Bi_2Sr_2CaCu_2O_{8+x}$. *Nature* **532**, 343–347 (2016).

[19] Tranquada, J. M. Cuprate superconductors as viewed through a striped lens. *Adv. Phys.* **69**, 437–509 (2020).

[20] Yang, H. B., Rameau, J. D., Johnson, P. D., Valla, T., Tsvelik, A. & Gu, G. D. Emergence of preformed Cooper pairs from the doped Mott insulating state in $Bi_2Sr_2CaCu_2O_{8+\delta}$. *Nature* **456**, 77–80 (2008).

[21] Li, L. *et al.* Diamagnetism and Cooper pairing above T_c in cuprates. *Phys. Rev. B* **81**, 054510 (2010).

[22] Bilbro, L. S., Aguilar, R. V., Logvenov, G., Pelleg, O., Bozovic, I. & Armitage, N.

P. Temporal correlations of superconductivity above the transition temperature in $La_{2-x}Sr_xCuO_4$ probed by terahertz spectroscopy. *Nat. Phys.* **7**, 298–302 (2011).

[23] Zhou, P. *et al.* Electron pairing in the pseudogap state revealed by shot noise in copper oxide junctions. *Nature* **572**, 493–496 (2019).

[24] Martin, S., Fiory, A. T., Fleming, R. M., Schneemeyer, L. F. & Waszczak, J. V. Normal-state transport properties of $Bi_{2+x}Sr_{2-y}CuO_{6+\delta}$ crystals. *Phys. Rev. B* **41**, 846 (1990).

[25] Gurvitch, M. & Fiory, A. T. Resistivity of $La_{1.825}Sr_{0.175}CuO_4$ and $YBa_2Cu_3O_7$ to 1100K: Absence of Saturation and Its Implications. *Phys. Rev. Lett.* **59**, 1337 (1987).

[26] Cooper, R. A. *et al.* Anomalous Criticality in the Electrical Resistivity of $La_{2-x}Sr_xCuO_4$. *Science* **323**, 603-607 (2009).

[27] Ayres, J. *et al.* Incoherent transport across the strange-metal regime of overdoped cuprates. *Nature* **595**, 661–666 (2021).

[28] Sachdev, S. & Keimer, B. Quantum criticality. *Phys. Today* **64**, 29 (2011).

[29] Damascelli, A., Hussain, Z. & Shen, Z. X. Angle-resolved photoemission studies of the cuprate superconductors. *Rev. Mod. Phys.* **75**, 473–541 (2003).

[30] Chen, S.-D. *et al.* Incoherent strange metal sharply bounded by a critical doping in Bi2212. *Science* **366**, 1099–1102 (2019).

[31] Maldacena, J. The Large N Limit of Superconformal field theories and supergravity. *Adv. Theor. Math. Phys.* **2**, 231–252 (1998).

[32] Hartnoll, S. A. Lectures on holographic methods for condensed matter physics. *Class. Quantum Gravity* **26**, 224002 (2009).

[33] Davison, R. A., Schalm, K. & Zaanen, J. Holographic duality and the resistivity of strange metals. *Phys. Rev. B* **89**, 245116 (2014).

[34] Lucas, A. & Hartnoll, S. A. Resistivity bound for hydrodynamic bad metals. *Proc. Natl. Acad. Sci. U. S. A.* **114**, 11344–11348 (2017).

[35] Zaanen, J. Planckian dissipation, minimal viscosity and the transport in cuprate strange metals. *SciPost Phys.* **6**, 061 (2019).

[36] Fujita, K. *et al.* Simultaneous transitions in cuprate momentum-space topology and electronic symmetry breaking. *Science* **344**, 612–616 (2014).

[37] Drozdov, I. K. *et al.* Phase diagram of $Bi_2Sr_2CaCu_2O_{8+\delta}$ revisited. *Nat. Commun.* **9**:5210 (2018).

[38] Hussey, N. E., Abdel-Jawad, M., Carrington, A., Mackenzie, A. P. & Balicas, L. A coherent three-dimensional Fermi surface in a high-transition-temperature superconductor. *Nature* **425**, 814–817 (2003).

[39] Vignolle, B. *et al.* Quantum oscillations in an overdoped high-T_c superconductor. *Nature* **455**, 952–955 (2008).

[40] Uemura, Y. J. *et al.* Magnetic-field penetration depth in $Tl_2Ba_2CuO_{6+\delta}$ in the overdoped regime. *Nature* **364**, 605–607 (1993).

[41] Lemberger, T. R., Hetel, I., Tsukada, A., Naito, M. & Randeria, M. Superconductor-to-metal quantum phase transition in overdoped $La_{2-x}Sr_xCuO_4$. *Phys. Rev. B* **83**, 140507 (2011).

[42] Bozovic, I., He, X., Wu, J. & Bollinger, A. T. Dependence of the critical temperature in overdoped copper oxides on superfluid density. *Nature* **536**, 309–311 (2016).

[43] Ohsugi, S., Kitaoka, Y. & Asayama, K. Temperature dependence of Spin Susceptibility of $La_{2-x}Sr_xCuO_4$. *Physica C* **282–287**, 1373–1374 (1993).

[44] Wang, Y. *et al.* Weak-coupling d -wave BCS superconductivity and unpaired electrons in overdoped $La_{2-x}Sr_xCuO_4$ single crystals. *Phys. Rev. B* **76,** 064512 (2007).

[45] Mahmood, F., He, X., Bozovic, I. & Armitage, N. P. Locating the Missing Superconducting Electrons in the Overdoped Cuprates $La_{2-x}Sr_xCuO_4$. *Phys. Rev. Lett.* **122,** 027003 (2019).

[46] Kondo, T. *et al.* Disentangling Cooper-pair formation above the transition temperature from the pseudogap state in the cuprates. *Nat. Phys.* **7**, 21–25 (2011).

[47] Kondo, T. *et al.* Point nodes persisting far beyond T_c in Bi2212. *Nat. Commun.* **6**:7699 (2015).

[48] He, Y. *et al.* Superconducting Fluctuations in Overdoped $Bi_2Sr_2CaCu_2O_{8+\delta}$. *Phys. Rev. X* **11**, 031068 (2021).

[49] Rourke, P. M. C. *et al.* Phase-fluctuating superconductivity in overdoped $La_{2-x}Sr_xCuO_4$. *Nat. Phys.* **7**, 455–458 (2011).

[50] Lee-Hone, N. R., Özdemir, H. U., Mishra, V., Broun, D. M. & Hirschfeld, P. J. Low energy phenomenology of the overdoped cuprates: Viability of the Landau-BCS paradigm. *Phys. Rev. Res.* **2**, 013228 (2020).

[51] Maier, T. A., Karakuzu, S. & Scalapino, D. J. The overdoped end of the cuprate phase diagram. *Phys. Rev. Res.* **2,** 033132 (2020).

[52] Spivak, B., Oreto, P. & Kivelson, S. A. d-Wave to s-wave to normal metal transitions in disordered superconductors. *Phys. B Condens. Matter* **404**, 462–465 (2009).

[53] Li, Z. X., Kivelson, S. A., & Lee, D. H. Superconductor-to-metal transition in overdoped cuprates *npj Quantum Mater.* **6**:36 (2021).

[54] Kopp, A., Ghosal, A. & Chakravarty, S. Competing ferromagnetism in high-temperature copper oxide superconductors. *Proc. Natl. Acad. Sci.* **104**, 6123–6127 (2007).

[55] Sonier, J. E. *et al.* Direct search for a ferromagnetic phase in a heavily overdoped nonsuperconducting copper oxide. *Proc. Natl. Acad. Sci.* **107**, 17131–17134 (2010).

[56] Li, X. *et al.* Quasiparticle interference and charge order in a heavily overdoped non-superconducting cuprate. *New J. Phys.* **20**, 063041 (2018).

[57] Peng, Y. Y. *et al.* Re-entrant charge order in overdoped $(Bi,Pb)_{2.12}Sr_{1.88}CuO_{6+\delta}$ outside the pseudogap regime. *Nat. Mater.* **17**, 697–702 (2018).

[58] Li, X. *et al.* Evolution of Charge and Pair Density Modulations in Overdoped $Bi_2Sr_2CuO_{6+\delta}$. *Phys. Rev. X* **11**, 011007 (2021).

[59] Fischer, Ø., Kugler, M., Maggio-Aprile, I., Berthod, C. & Renner, C. Scanning tunneling spectroscopy of high-temperature superconductors *Rev. Mod. Phys.* **79**, 353–419 (2007).

[60] Hoffman, J. E. Spectroscopic scanning tunneling microscopy insights into Fe-based superconductors. *Reports Prog. Phys.* **74**, 124513 (2011).

[61] Yazdani, A., Da Silva Neto, E. H. & Aynajian, P. Spectroscopic Imaging of Strongly Correlated Electronic States. *Annu. Rev. Condens. Matter Phys.* **7**, 11–33 (2016).

[62] Binnig, G. & Rohrer, H. Scanning Tunneling Microscopy—from Birth to Adolescence (Nobel Lecture). *Rev. Mod. Phys.* **59**, 615 (1987).

[63] Chen, C. J. *Introduction to Scanning Tunneling Microscopy.* (Oxford University Press, 2000).

[64] Battisti, I., Verdoes, G., Van Oosten, K., Bastiaans, K. M. & Allan, M. P. Definition of design guidelines, construction, and performance of an ultra-stable scanning tunneling microscope for spectroscopic imaging. *Rev. Sci. Instrum.* **89**, 123705 (2018).

[65] Crommie, M., Lutz, C. & Eigler, D. Imaging standing waves in a 2D electron gas *Nature* **363**, 524–527 (1993).

[66] Petersen, L. *et al.* Direct imaging of the two-dimensional Fermi contour: Fourier-transform STM *Phys. Rev. B* **57**, R6858 (1998).

[67] Wang, Z. *et al.* Quasiparticle interference and strong electron-mode coupling in the quasi-one-dimensional bands of Sr_2RuO_4. *Nat. Phys.* **13**, 799–805 (2017).

[68] Li, H. *et al.* Rotation symmetry breaking in the normal state of a kagome superconductor KV_3Sb_5 *Nat. Phys.* **18**, 265–270 (2022).

[69] Hoffman, J. E. *et al.* Imaging Quasiparticle Interference in $Bi_2Sr_2CaCu_8$ *Science* **297**, 1148–1151 (2002).

[70] Allan, M. P. *et al.* Anisotropic Energy Gaps of Iron-Based Superconductivity from Intraband Quasiparticle Interference in LiFeAs. *Science* **336**, 563–567 (2012).

[71] Coleman, P. *Introduction to Many-body Physics*. (Cambridge University Press, 2015).

[72] Hufner, S. *Photoelectron Spectroscopy*. (Springer-Verlag, 2003).

[73] Sulangi, M. A. & Zaanen, J. Self-energies and quasiparticle scattering interference. *Phys. Rev. B* **98**, 094518 (2018).

[74] Feenstra, R. M., Stroscio, J. A. & Fein, A. P. Tunneling spectroscopy of the Si(111)2×1 surface. *Surf. Sci.* **181**, 295–306 (1987).

[75] Macdonald, A. J. *et al.* Dispersing artifacts in FT-STS: A comparison of set point effects across acquisition modes. *Nanotechnology* **27**, 414004 (2016).